Available online at www.sciencedirect.com
SCIENCE DIRECT®
ELSEVIER
Journal of Magnetism and Magnetic Materials 268 (2004) 95–104
journal of magnetism and magnetic materials
www.elsevier.com/locate/jmmm

Nanophase formation of strontium hexaferrite fine powder by the sonochemical method using $Fe(CO)_5$

M. Sivakumar[a], A. Gedanken[a,*], W. Zhong[b], Y.W. Du[b], D. Bhattacharya[c], Y. Yeshurun[c], I. Felner[d]

[a] *Department of Chemistry, Bar-Ilan University, Ramat-Gan 52900, Israel*
[b] *National Laboratory of Solid State Microstructures, Nanjing University, Nanjing 210093, People's Republic of China*
[c] *Department of Physics, Institute of Superconductivity, Bar-Ilan University, Ramat-Gan, Israel, 52900*
[d] *The Racah Institute of Physics, The Hebrew University, Jerusalem 91904, Israel*

Received 9 March 2003; received in revised form 7 May 2003

Abstract

A fine strontium hexaferrite powder has been successfully synthesized by a sonochemical method employing $Fe(CO)_5$ and $SrCO_3$. $SrCO_3$ was first synthesized using strontium nitrate and urea, and it was found that applying ultrasound radiation during this process results in the uniform formation of $SrCO_3$ hexagonal rods. These rods were then dispersed with in situ generated amorphous Fe_2O_3, using $Fe(CO)_5$ as the source. The resultant precursor was then calcined at 900°C, which is lower than the conventional solid-state reaction of applying 1300°C to get the strontium hexaferrite fine powder. This sonochemically derived ferrite exhibited an intrinsic coercivity of ~4600 Oe and a saturation magnetization of ~60 emu/g at 20 K and ~32 emu/g at 300 K.

PACS: 75.50.Tt; 81.07.Bc; 75.75.+a

Keywords: Sonochemistry; Cavitation; Magnetic; Nanomaterial; Hexaferrite

1. Introduction

The hexagonal M-type hard hexaferrites have attracted much attention as the most widely used permanent magnets, which account for about 90 wt% of the annual production of permanent magnets. Strontium hexaferrite, $SrFe_{12}O_{19}$, is a ferrimagnet in which iron ions in five different crystallographic sites are coupled antiferromagnetically. This ferrimagnet exhibits a high saturation magnetization and high coercivity because of the relatively high magnetocrystalline anisotrophy field [1]. This ferrite has been explored for many technologically demanding and challenging applications, such as for permanent magnets and high-density perpendicular recording media, with proper doping [2]. The properties of this ferrite are largely dependent on the processing routes used for its fabrication [1,3]. Traditionally, this ferrite powder is synthesized by a mixed oxide ceramic

*Corresponding author. Tel.: +97235318315; fax: +97235351250.
E-mail address: gedanken@mail.biu.ac.il (A. Gedanken).

0304-8853/03/$ - see front matter © 2003 Elsevier B.V. All rights reserved.
doi:10.1016/S0304-8853(03)00479-7

method, which involves the solid-state reaction between $SrCO_3$ and Fe_2O_3 at a high calcination temperature ($\sim 1300^\circ C$) [4]. However, this technique has the disadvantage of resulting in larger particle size and agglomerates and uncontrolled particle morphology. Also, the subsequent milling of the calcined ferrite powder undoubtedly introduces a level of contamination and, therefore, degrades the magnetic properties [5].

Thus, the preparation of strontium ferrite powder with refined particle size, narrowed particle size distribution, and minimal particle agglomeration has received considerable attention [6]. In order to improve the material properties, numerous nonconventional soft synthetic routes have been devised, including co-precipitation [7–10], hydrolysis of metalorganic complexes [11], sol–gel synthesis [12–14], spray pyrolysis [15], the citrates method [2,12,14], glass crystallization [16–19] and hydrothermal reaction [20–22]. Ultrafine strontium ferrite powder with particle sizes in the range of ~ 50 nm have been prepared successfully via some of these processing routes, but the magnetic properties of the resulting ferrite powders vary considerably from one material to another. For example, Choy et al. [12] reported a coercive force of 6500 Oe for one of the strontium ferrite powders prepared via a sol–gel processing route, although the powder exhibits a relatively low magnetization (50 emu/g).

One of the major difficulties encountered in many of these wet-chemistry-based processing routes for strontium ferrites, such as in co-precipitation [8,23] and in hydrothermal reaction, is the relatively low solubility of $Sr(OH)_2$ in an aqueous solution. This low solubility poses problems in maintaining the stoichiometry of the strontium ferrite, although excess strontium can be introduced into the starting composition. For example, a Sr^{+2}:Fe^{+3} ratio of 1:11 was used by Kulkarni et al. [8] in their co-precipitation route, in comparison with the stoichiometry ratio of 1:12 in $SrFe_{12}O_{19}$.

Application of ultrasound for the synthesis of newer materials has become an attractive area in recent times. Cavitation is the phenomenon that underlines the effects observed during the passage of ultrasound. This includes the formation, growth and implosive collapse of the cavities. This produces extreme conditions of temperature ($\sim 5000^\circ C$), pressure (~ 20 Mpa), and cooling rates ($> 10^{10}$ K/s), which lead to many unusual and unique physical and chemical effects. Recently, the cavitational collapse effects have been effectively used to prepare nanoscale metals, metal oxides, and nanocomposites [24,25].

In the current research, we report on a new method for the synthesis of single phase, ultrafine, $SrFe_{12}O_{19}$ particles. The method makes use of ultrasound irradiation in two stages: (i) to synthesize uniform rods of $SrCO_3$, (ii) decomposing $Fe(CO)_5$ and dispersing the in situ formed amorphous Fe_2O_3 on the prepared $SrCO_3$ obtained in the first stage to get the precursor. Calcinating this precursor then results in the formation of a fine hexaferrite powder.

2. Experimental section

2.1. Starting materials

The starting materials used in the present work included strontium nitrate hexahydrate (Aldrich, 99%), urea (Aldrich, 98%), $Fe(CO)_5$ (Strem chemicals, USA, 99.5%), decalin (Acros organics, 98%) and pentane (96%, Bio-lab, Israel).

2.2. Preparation procedures

2.2.1. Stage 1: preparation of $SrCO_3$

The synthesis of strontium carbonate particles was carried out with the aid of ultrasound radiation. About 5 g of urea was added to an aqueous solution (50 ml) of 1.0 g of strontium nitrate hexahydrate in a sonication flask. The solution was then irradiated for 3 h with high intensity ultrasound radiation by employing a direct immersion titanium horn (Sonics and Materials, 20 kHz, 600 W). Calorimetry was used to estimate the electroacoustic or energy transfer efficiency of the transducer to the solution. Based on the calorimetry experiments, the transfer efficiency of the ultrasonic energy from the transducer to the reactor solution was estimated as 54% (at 65% amplitude), with the assumption

that all ultrasonic energy was converted to heat in the reactor. Based on these calorimetry measurements, the power intensity of the system was calculated as 29.7 W/cm^2. The titanium horn tip was inserted into the solution to a depth of 1 cm. The temperature during the experiment increased to a maximum of 85°C due to ultrasound passage, as measured by an iron Constantan thermocouple. After the precipitation process was complete, the precipitates were separated from the solution by centrifugation. The recovered precipitate was then washed several times with doubly distilled water and dried under vacuum at room temperature.

2.2.2. Stage 2: dispersion of amorphous Fe_2O_3 obtained from $Fe(CO)_5$ on $SrCO_3$

This step utilizes the principle of obtaining pure amorphous materials from suitable precursors by means of sonication [24,26]. The preparation of amorphous Fe_2O_3 was reported elsewhere [26]. Following the same principle, the present process involves taking stoichiometric amounts of $SrCO_3$ and $Fe(CO)_5$ in decalin and irradiating the solution with ultrasound (the method followed is similar to stage 1). The reaction was carried out in an air atmosphere at 0°C for 4 h. After 4 h, the obtained product was thoroughly washed with pentane, centrifuged, and dried in vacuum at room temperature. The product thus obtained will hereafter be referred to as the precursor. This precursor was calcined at 900°C for 14 h in air atmosphere to obtain strontium hexaferrite fine powder.

2.3. Characterization

The phase constitution of the hexaferrite powder was recorded by employing a Rigaku X-ray diffractometer (Model-2028, Co Kα). XRD measurements were taken in the scanning range: 2θ from 15° to 70°. The microstructures of the products were determined by transmission electron microscopy (TEM) (JEOL-JEM 100SX microscope). The powder morphology was also examined by a scanning electron microscope (JEOL-JSM-840). Samples for TEM were prepared by placing a drop of the sample suspension on a copper grid coated with carbon (400 mesh, electron microscopy sciences) and allowing them to dry in air. FT-IR spectra were recorded on a Nicolet (Impact 410) infrared spectrophotometer with KBr pellets over the range of $400 \pm 3000\,\mathrm{cm}^{-1}$. The thermogravimetric analysis was performed in an oxygen atmosphere using a Mettler Toledo TGA/SDTA851 instrument attached to a mass spectrometer (Balzers Instruments), over the temperature range of 30–1000°C (heating rate ~10°C/min). Complex permeability spectra were measured with a coaxial transmission line connected to an impedance analyzer (Agilent4284A from 20 Hz to 1 MHz), or an impedance/material analyzer (Agilent4191B from 1 MHz to 1.8 GHz). The magnetic measurements were performed over a wide temperature range of 20–900 K. The magnetization vs. temperature, as well as hysteresis loops at different temperatures, within the temperature range 20–300 K, were measured in a SQUID magnetometer coupled with a superconducting magnet (MPMS-5S, Quantum Design). The high-temperature magnetic properties were measured in a vibrating sample magnetometer coupled with a furnace attachment (Oxford).

3. Results and discussion

3.1. XRD

The $SrCO_3$ sample synthesized by ultrasound irradiation in stage 1 shows a crystalline X-ray pattern (Fig. 1a), which matches that reported for standard $SrCO_3$. Fig. 1c illustrates the XRD pattern of the precursor product obtained by sonicating the decalin solution of $Fe(CO)_5$ and $SrCO_3$. The XRD pattern of this precursor is very similar to the pattern of Fig. 1a except that it has an amorphous background in addition to the $SrCO_3$ peaks. This is due to the application of ultrasound on the $Fe(CO)_5$, which generates amorphous Fe_2O_3. The amorphous Fe_2O_3 was then dispersed or coated on $SrCO_3$ again with the assistance of ultrasound. In order to confirm this, a solution of $Fe(CO)_5$ in decalin alone was sonicated at 0°C for 4 h. Fig. 1b shows the XRD

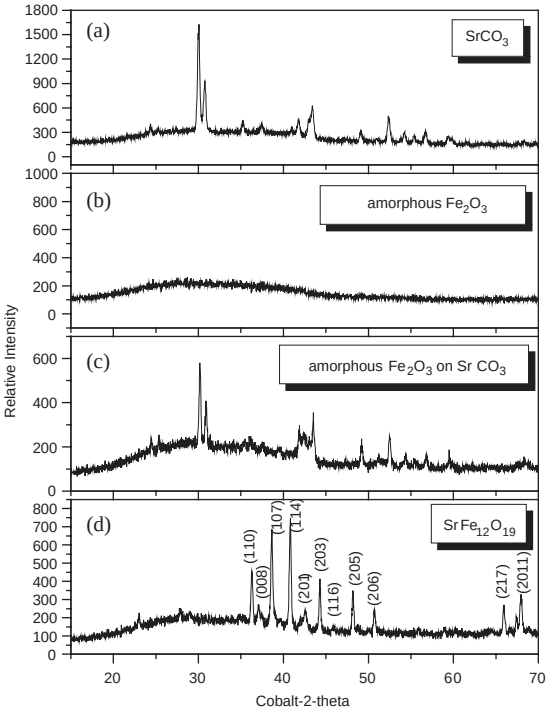

Fig. 1. Powder X-ray diffraction patterns of the (a) as-synthesized $SrCO_3$, (b) amorphous Fe_2O_3 (for comparison), (c) amorphous Fe_2O_3 dispersed on $SrCO_3$, and (d) $SrFe_{12}O_{19}$ obtained by calcining the precursor at 900°C in air for 14 h.

pattern of the resultant product obtained during this process. It can be seen from this pattern that the Fe_2O_3 obtained in this process is amorphous. Fig. 1d shows the XRD pattern of $SrFe_{12}O_{19}$ obtained by calcining the precursor sample at 900°C in air atmosphere for 14 h. The diffraction peaks match those reported for standard $SrFe_{12}O_{19}$. Heating the precursor at a rate of 8°C/min to 900°C resulted in a well-crystallized ferrite phase. This was indicated by the appearance of the most intense reflections (1 1 4), (1 0 7) and (1 1 0) peaks at 2θ angles of 40.86°, 38.63° and 36.28° respectively, as shown in Fig. 1d. Thus, the formation of $SrFe_{12}O_{19}$ is completed at 900°C. Also, the formation temperature for $SrFe_{12}O_{19}$ by the sonochemically prepared precursor is apparently lower than that observed in the conventional solid-state reaction utilizing $SrCO_3$ and Fe_2O_3 (~1300°C) and in the precursors obtained via spray pyrolysis (~1200°C) for forming a single phase of $SrFe_{12}O_{19}$. Thus, the formation temperature of $SrFe_{12}O_{19}$ by this process compares reasonably well with many other chemistry-based processing routes.

3.2. TGA

TGA results for the as-synthesized strontium carbonate in stage 1 are shown in Fig. 2a. The only weight loss that can be observed is between 900°C and 1000°C. This weight loss may be ascribed to the carbonate decomposition. Fig. 2b depicts the TGA curve for the as-synthesized precursor in stage 2. The TGA shows three distinct weight loss steps. All these three steps are confined to the weight loss stages of amorphous Fe_2O_3, as from Fig. 2a it can be seen that $SrCO_3$ gives a weight loss only in between 900°C and 1000°C. It can also be noted from Fig. 2b that due to the deposition of amorphous Fe_2O_3 on $SrCO_3$, the temperature of the final weight loss for the precursor completes around 900°C. For comparison, Fig. 2c shows the TGA curve for the sonochemical as-synthesized amorphous Fe_2O_3 obtained by the decomposition of $Fe(CO)_5$.

This curve matches that of the precursor (Fig. 2b) for amorphous Fe_2O_3 weight loss stages. Also, it has already been found that by heating the amorphous Fe_2O_3 around 300°C, it loses its amorphous character and converts into crystalline material [26].

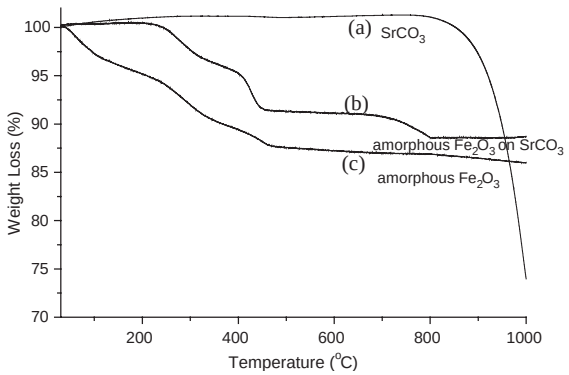

Fig. 2. TGA results of the as-synthesized $SrCO_3$, amorphous Fe_2O_3 (for comparison) and precursor (amorphous Fe_2O_3 dispersed on $SrCO_3$)

3.3. Mössbauer investigations

As a confirmation of the phase purity, Fig. 3 shows the ^{57}Fe Mössbauer spectrum at 300 K for the $SrFe_{12}O_{19}$ powder calcined at 900°C for 14 h in air atmosphere. Dots in this figure represent the experimental data points, while the solid lines are the least-squares fitting for these data. Generally speaking, this complicated spectrum is composed of five sub-spectra corresponding to the five inequivalent crystallographic sites of Fe in this hexagonal ferrite material. Unfortunately, there is considerable controversy regarding the five hyperfine fields in this material. We adopted the interpretation and the values suggested by Evans et al. [27]. The isomer shifts and the hyperfine fields obtained are in excellent agreement with the data already obtained [27] and for the sake of brevity they have not been listed and discussed here. Thus, this spectrum fits reasonably well with the spectrum of the standard $SrFe_{12}O_{19}$ phase and clearly indicates that the material measured is indeed $SrFe_{12}O_{19}$.

3.4. Permeability spectra

A useful route to investigate the mechanism of domain wall motions and domain rotations is to measure the complex permeability as a function of frequency, i.e., the so-called magnetic spectrum. In addition, by studying such a magnetic spectrum, the effective magnetic anisotropy field, as well as damping mechanism of domain wall displacements, can be checked. In general, the dispersions caused by wall displacements occur in radio frequency range (below 10 MHz), and those caused by domain rotations often appear in the microwave range (100 MHz to 10 GHz). In particular, this methodology has been extensively used in ferrites [28,29]. Thus, a similar study has been carried out in the $SrFe_{12}O_{19}$ powder prepared by the present ultrasonic method and calcined at 900°C for 14 h in air atmosphere.

The frequency dependence of the real part μ' and imaginary part μ'' of complex permeability spectra is shown in Fig. 4. For permeability measurements, the nanosized $SrFe_{12}O_{19}$ powder sample was pressed into a ring with a typical size of 13 mm OD, 7 mm ID and 1 mm thickness. The pressed ring has a lower density than the sintered sample. According to the theory contemplation, in single-domain grains, there are no domain wall motions. Therefore, the μ_0 (static permeability, i.e. μ' with frequency limit to zero) is only caused by reversible domain rotations and follows the relation $\mu_0 = 1 + 8\pi M_s/3H_a$, where H_a is the effective magnetic anisotropy field. Because the H_a of $SrFe_{12}O_{19}$ is very large (8100 Oe), the complex permeability is small. From Fig. 4, one can see that the μ' is about 1.2, smaller than the theory prognosis. We think that the nonmagnetic impurities

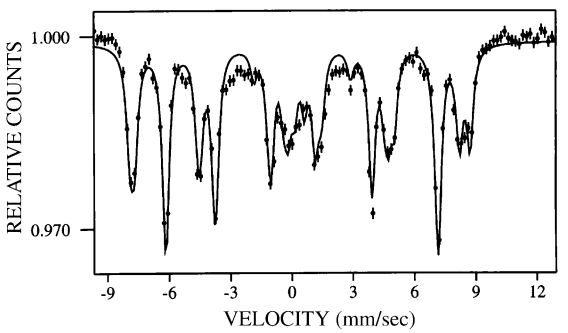

Fig. 3. Mössbauer spectra of the $SrFe_{12}O_{19}$ obtained by calcining the precursor at 900°C in air atmosphere for 14 h. (•) indicates the experimental points and the (—) is the theoretical fitting.

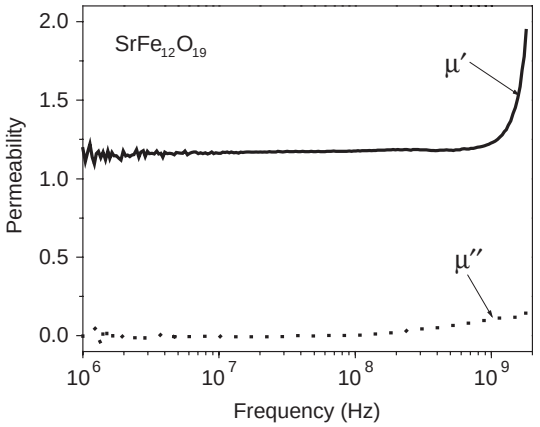

Fig. 4. The plots of complex permeability as a function of frequency for the polycrystalline $SrFe_{12}O_{19}$ sample at room temperature.

such as boundaries, and cavities resulting from the low-density structure, may cause the permeability to decline further. In the corresponding bulk sample, there are domain wall motions, whereas in nanosized sample, there are only reversible domain rotations. The μ_0 contributed by domain rotations is generally smaller than that by domain wall displacements.

3.5. IR spectra

The IR spectra of Figs. 5a and c provide evidence for the presence of carbonate ions in $SrCO_3$ and in the precursor, respectively. The strong absorption band at 1470 cm^{-1} in the case of as-synthesized $SrCO_3$ and 1469 cm^{-1} in the case of precursor had been attributed to the v_3 mode of the CO_3^{2-} ion of $SrCO_3$.

The other bands around 850 and 700 cm^{-1} are assigned to the v_2 and v_4 modes of the carbonate ion, respectively. The IR spectrum of the amorphous Fe_2O_3 synthesized by ultrasound alone (for comparison) shows absorption bands at 473, 1424 and 1550 cm^{-1} in Fig. 5b.

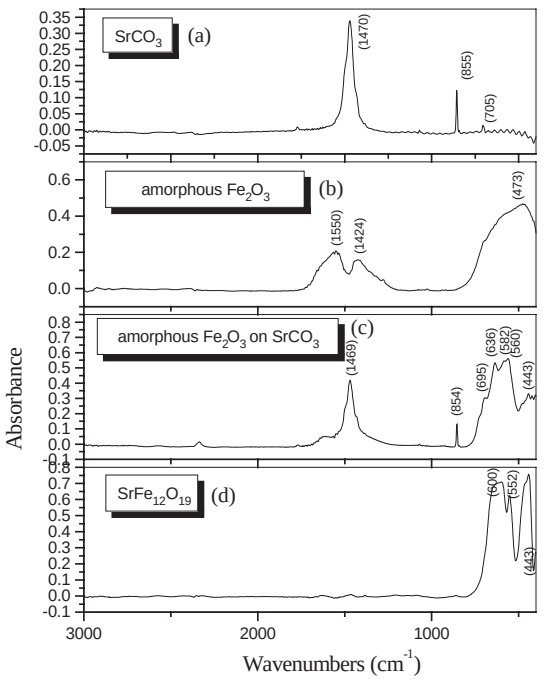

Fig. 5. IR spectra of the (a) as-synthesized $SrCO_3$, (b) amorphous Fe_2O_3 (for comparison), (c) amorphous Fe_2O_3 dispersed on $SrCO_3$, and (d) $SrFe_{12}O_{19}$ obtained by calcining the precursor at 900°C in air for 14 h.

Well-established absorption bands in Fig. 5d at 443, 552 and 600 cm^{-1} in the powder calcined at 900°C indicate the formation of strontium ferrite. Meanwhile, the characteristic bands of $SrCO_3$ and iron oxides vanish at this calcination temperature. The disappearance of the carbonate peaks provides unequivocal proof for the lowering of the sintering temperature from 1200°C to 900°C. The above interpretation of the IR spectral results is based on the assumption that the synthesized carbonate, Fe_2O_3, precursor and hexaferrite are essentially pure materials. These results agree with the XRD phase-analysis findings.

3.6. TEM

Fig. 6a shows the results of TEM investigation of the synthesized strontium carbonate using ultrasound. It can be clearly seen from this picture that ultrasound promotes the homogeneous formation of rods and their average diameter and length are 1.2 and 8 μm, respectively. Fig. 6b depicts the TEM picture of the amorphous Fe_2O_3 powder dispersed on the hexagonal $SrCO_3$ rods. It is clearly seen that there is no crystalline formation of Fe_2O_3 in this powder. It can also be observed that this amorphous Fe_2O_3 is an agglomerate of small particles aggregated in a spongelike form.

Fig. 6c micrograph indicates the morphology of the ferrite sample typical of the M-ferrites obtained after treating it at 900°C. It can be observed from this micrograph that after calcination, the ferrite particles have an average diameter of about 50 nm. No remaining $SrCO_3$ and Fe_2O_3 could be observed in the micrograph in spite of the low heat treatment temperature. This result agrees with the results of XRD and IR.

3.7. Measurement of the magnetic properties

The magnetization vs. temperature pattern over the entire temperature range is shown in Fig. 7. From this plot, one extracts the Curie point to be ~800 K. Hysteresis loops at 20 and 300 K are shown in the inset of Fig. 7. From the hysteresis

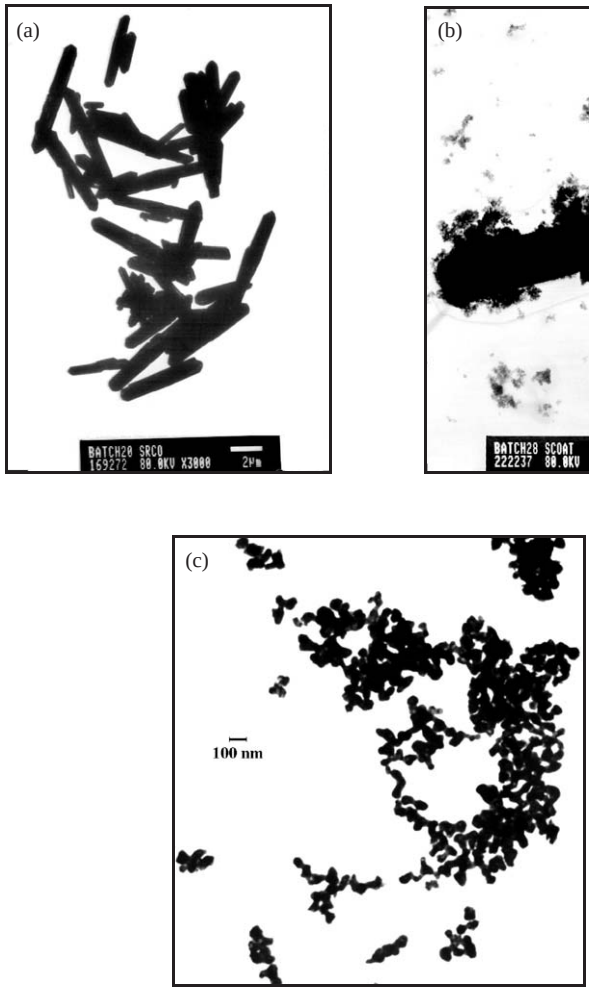

Fig. 6. TEM of (a) as-synthesized $SrCO_3$, (b) amorphous Fe_2O_3 dispersed on $SrCO_3$, and (c) $SrFe_{12}O_{19}$, obtained by calcinating the precursor b at 900°C in air for 14 h.

loop, we extract the coercive field (H_c) and the saturation magnetization (M_s). The H_c and M_s values are found to be $\sim$4600 Oe and $\sim$60 emu/g, respectively, at $\sim$20 K. While the M_s value drops down with temperature and, at room temperature (300 K), it becomes $\sim$32 emu/g, the H_c value remains more or less temperature independent over the 20–300 K range. Other pertinent data are the remanence magnetization (M_r) and the loop squareness ratio (M_r/M_s); they are found to be $\sim$45 emu/g and $\sim$0.8, respectively, at 20 K and $\sim$19 emu/g and $\sim$0.6, respectively, at 300 K. It is interesting to note that the magnetization vs. temperature pattern exhibits a strong temperature dependence over a range of 300–800 K. This could be because of the presence of single-domain nanoparticles and consequent superparamagnetism over this temperature range.

At a lower temperature, however, magnetization tends towards saturation, possibly because of the fact that the blocking temperature (T_B) is crossed, which helps in restoring the bulk magnetization behavior. The T_B could be around 300 K. The Curie point (T_c) extracted from the high-temperature magnetization vs. temperature pattern ($\sim$800 K) appears to be higher than the bulk

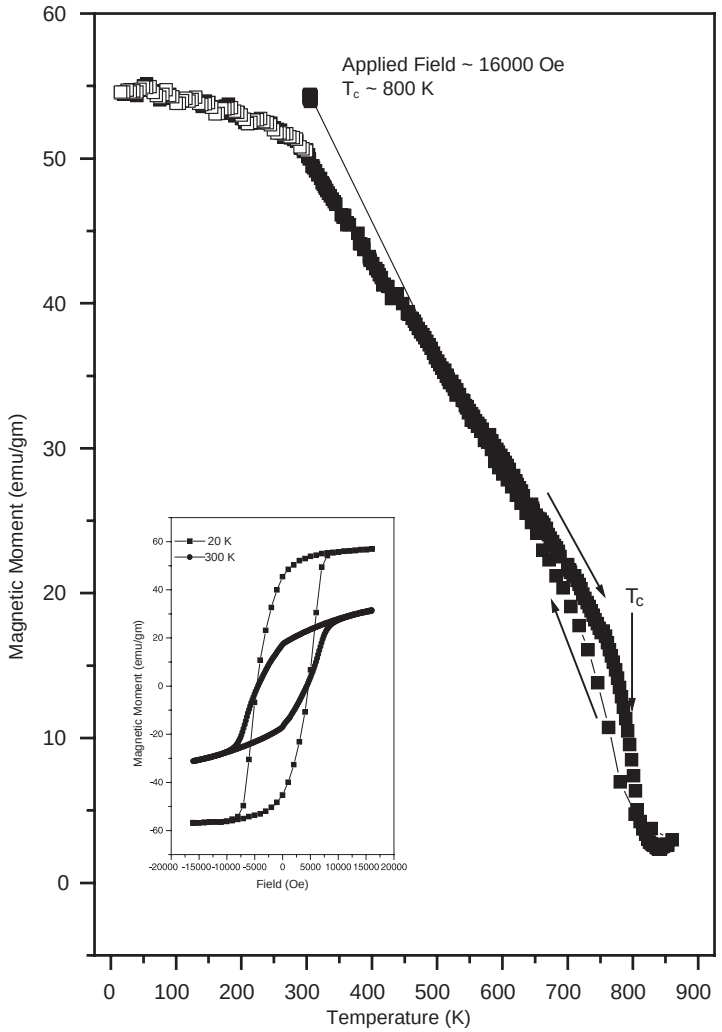

Fig. 7. The magnetization vs. temperature pattern over the temperature ranges 20–900 K for the ultrafine $SrFe_{12}O_{19}$ system prepared by a sonochemical technique followed by calcination at 900°C for 14 h. Hysteresis loops measured at 20 and 300 K are shown in the inset.

Curie point ~750 K. This result corroborates the already obtained observation [30], where a rise in T_c as a function of drop in particle size is reported. The magnetization (M) vs. field (H) curve, especially at higher temperature, is not found to be pure Langevin-type due to the distribution of the randomly oriented anisotropy axes.

It is known that magnetic properties such as saturation magnetization and the magnetic hyperfine field value of nanoparticles are much smaller than those of the corresponding bulk materials. The energy of a magnetic particle in an external field is proportional to its size or volume via the number of magnetic molecules in a single magnetic domain. When this energy becomes comparable to thermal energy, thermal fluctuations will significantly reduce the total magnetic moment at a given field [31]. Another reason for the reduced magnetization could be the large surface-to-volume ratio for small particles. The magnetic molecules on the surface lack complete co-ordination, and the spins are also disordered. As a result of this, we observe

a drop in saturation magnetization value comparable to the single crystal data ($M_s = 68$ emu/gm). This result, therefore, provides evidence of the presence of ultrafine particles in the sample. However, the coercive field value (~ 4600 Oe) too exhibits a drop, in comparison with the theoretical value predicted for a single crystal (~ 7500 Oe) [7]. Whereas strontium ferrite powders from an ethanol-based microemulsion show a maximum coercivity value of 6195 Oe [32], single-domain strontium hexaferrite particles obtained by a modified co-precipitation method also show a high coercivity value of 5550 Oe [33]. Thus, the low value of the coercive field obtained in the present case can be due to the low crystalline anisotropy, which arises from crystal imperfection and a high degree of aggregation.

4. Results and discussion

The role of urea in the homogeneous precipitation of strontium carbonate particles (as synthesized in stage 1) is that it decomposes by hydrolysis homogeneously in the solution upon heating, producing CO_2, OH^- and NH_4^+ ions in the solution. This increases the pH of the medium, which is suitable for the formation of strontium carbonate particles. Measurement of the pH before and after the sonication experiment revealed that the pH of the solution increased from 5.4 to 6.2. Applying ultrasound radiation during the reaction might accelerate the homogeneous precipitation process. In addition to this, it might also be beneficial in controlling the particle size and the shape.

In the conventional solid-state reaction of Fe_2O_3 with $SrCO_3$ to form the hexaferrite, the major limitation is the diffusion factor. In the present sonochemical method, this diffusion resistance may be overcome as there is an in situ generation of amorphous Fe_2O_3 from $Fe(CO)_5$ by ultrasound, followed by its dispersion or deposition on $SrCO_3$, assisted again by ultrasound. This process might facilitate the diffusion, as well as the reaction, of highly reactive strontium ion (Sr^{+2}) with the amorphous Fe_2O_3, resulting in the completion of the phase transition of the precursor to the $SrFe_{12}O_{19}$ hexaferrite at a lower calcination temperature of 900°C, employed in the present method.

The amorphous nature of Fe_2O_3 synthesized by ultrasound might also play a key role in increasing its reactivity with $SrCO_3$, resulting in the formation of a hexaferrite phase at the lower calcination temperature. The importance of amorphicity in increasing the reactivity has already been discussed [34]. Suslick et al. [34] have clearly shown that sonochemically prepared amorphous Fe, Co and Fe–CO nanomaterials are better catalysts than the corresponding crystalline nanomaterials prepared by other methods. In addition, Yee et al. [35] have functionalized amorphous Fe_2O_3 nanoparticles with alkanesulfonic and octadecanephosphonic acids. This work further supports the fact that it is possible to form a coating of organic molecules more easily on amorphous Fe_2O_3. In addition to the above factors, the size of the reactants (in specific, nanocrystalline amorphous Fe_2O_3) also contributes to the lowering of calcination temperature. It can be seen from the work of Ataie and Heshmati-Manesh that by using conventional strontium and iron nitrates, the mean particle size of the ferrite obtained is about 225 nm, at a calcination temperature of 900°C [33]. In the present case, however, by applying the same calcination temperature of 900°C, the mean particle size of the obtained ferrite is 50 nm, which might be due to amorphous Fe_2O_3 already present in the reacting system.

5. Conclusions

To summarize, we have demonstrated a novel sonochemical method for the synthesis of well-crystallized monophasic $SrFe_{12}O_{19}$ fine particles by the decomposition of $Fe(CO)_5$, followed by its reaction with $SrCO_3$, the synthesis of which was again assisted by ultrasound. More importantly, by this sonochemical method, formation of the $SrFe_{12}O_{19}$ single phase occurs at a temperature as low as 900°C. It should also be noted that similar results, as reported here for the $SrFe_{12}O_{19}$ synthesis, should be expected for $BaFe_{12}O_{19}$ due to their similar chemical behavior.

Acknowledgements

We thank The Ministry of Science, Sport and Culture for a Materials Science grant through the Sino-Israeli program in Materials Science. We also thank Ms. Louise Braverman for editorial assistance.

References

[1] H. Kojima, in: E.P. Wohlfarth (Ed.), Ferromagnetic Materials: A Handbook on the Properties of Magnetically Ordered Substances, Vol. 3, North-Holland, Amsterdam, 1982.
[2] P. Hernandez, C. de Francisco, J.M. Munoz, J. Iniguez, L. Torres, M. Zazo, J. Magn. Magn. Mater. 158 (1996) 123.
[3] H. Stablein, in: E.P. Wohlfarth (Ed.), Ferromagnetic Materials: A Handbook on the Properties of Magnetically Ordered Substances, Vol. 3, North-Holland, Amsterdam, 1982.
[4] F. Haberey, A. Kockel, IEEE Trans. Magn. 12 (1976) 983.
[5] S. Blackburn, T.P. Johnson, C.B. Ponton, M.H.L. Wise, Trans. Inst. Chem. Eng. 73 (Part A) (1995) 71.
[6] Z. Jin, W. Tang, J. Zhang, H. Lin, Y. Du, J. Magn. Magn. Mater. 182 (1993) 231.
[7] V.V. Pankov, M. Pernet, P. Germi, P. Mollard, J. Magn. Magn. Mater. 120 (1993) 69.
[8] S. Kulkarni, J. Shrotri, C.E. Deshpande, S.K. Kate, J. Mater. Sci. 24 (1989) 3739.
[9] S.E. Jacobo, C. Domingo-Pascual, R. Rudriguez-Clemente, M.A. Blesa, J. Mater. Sci. 32 (1997) 1025.
[10] W. Roos, J. Am. Ceram. Soc. 63 (1980) 601.
[11] K. Haneda, C. Miyakawa, K. Goto, IEEE Trans. Magn. 23 (1987) 3134.
[12] J.-H. Choy, Y.-S. Han, S.-W. Song, Mater. Lett. 19 (1994) 257.
[13] C. Surig, K.A. Hempel, D. Bonnenberg, Appl. Phys. Lett. 63 (1993) 2836.
[14] R. Ardiaca, R. Ramos, A. Isalgue, J. Rodriguez, X. Obradors, M. Pernet, M. Vallet, IEEE Trans. Magn. 23 (1987) 22.
[15] Y. Senzaki, J. Caruso, M.J. Hampden-Smith, T.T. Kodas, L.-M. Wang, J. Am. Ceram. Soc. 78 (1995) 2973.
[16] H. Sato, T. Umeda, Mater. Trans. JIM. 34 (1993) 76.
[17] D. Bahadur, D. Chakravorty, J. Mater. Sci. 32 (1997) 189.
[18] K. Oda, T. Yoshio, K.O. Oka, F. Kanamaru, J. Mater. Sci. Lett. 3 (1984) 1007.
[19] O. Kubo, T. Ido, H. Yokoyama, IEEE Trans. Magn. 18 (1982) 1122.
[20] J.H. Lee, H.S. Kim, C.W. Won, J. Mater. Sci. Lett. 15 (1996) 295.
[21] A. Ataie, I.R. Harris, C.B. Ponton, J. Mater. Sci. 30 (1995) 1429.
[22] C.H. Lin, Z.W. Shih, T.S. Chin, M.L. Wang, Y.C. Yu, IEEE Trans. Magn. 26 (1990) 15.
[23] A. Ataie, I.R. Harris, C.B. Ponton, in: J. David (Ed.), Introduction to Magnetism and Magnetic Materials, Chapman & Hall, London, 1991.
[24] K.S. Suslick, S.B. Choe, A.A. Cichowlas, M.W. Grinstaff, Nature 353 (1991) 414.
[25] K.S. Suslick, M. Fang, T. Hyeon, A.A. Cichowlas, in: K.E. Gonslaves, G.M. Chow, T.O. Xiao, R.C. Cammarata (Eds.), Molecularly Designed Ultrafine Nanostructured Materials, Materials Research Society, Pittsburgh, PA, 1994.
[26] X. Cao, Yu. Koltypin, R. Prozorov, G. Kataby, A. Gedanken, J. Mater. Chem. 12 (1997) 2447.
[27] B.J. Evans, F. Grandjen, A.P. Lilot, R.H. Vogel, A. Gerard, J. Magn. Magn. Mater. 67 (1987) 123.
[28] G.T. Rado, R.W. Wright, W.H. Emerson, Phys. Rev. 80 (1950) 273.
[29] G.T. Rado, R.W. Wright, W.H. Emerson, A. Terris, Phys. Rev. 88 (1952) 909.
[30] A. Vijayalakshmi, N.S. Gajbhiye, J. Appl. Phys. 83 (1998) 400.
[31] K.V.P.M. Shafi, A. Gedanken, R. Prozorov, J. Balogh, Chem. Mater. 10 (1998) 3445.
[32] J. Fang, J. Wang, L-M. Gan, S-C. Ng, J. Ding, X. Liu, J. Am. Ceram. Soc. 83 (2000) 1049.
[33] A. Ataie, S. Heshmati-Manesh, J. Eur. Ceram. Soc. 21 (2001) 1951.
[34] K.S. Suslick, T. Hyeon, M. Fang, Chem. Mater. 8 (1996) 2172.
[35] C. Yee, G. Kataby, A. Ulman, T. Prozorov, H. White, A. King, M. Rafailovich, J. Sokolov, A. Gedanken, Langmuir 15 (1999) 7111.